Y. Xie, S.-S. Li, Y.-W. Lin, Z. Ren, and C. T.-C. Nguyen, "Spurious mode suppression in UHF micromechanical extensional wine-glass ring resonators," *Proceedings*, 18th Int. IEEE Micro Electro Mechanical Systems Conf., Miami, Florida, Jan. 30 - Feb. 3, 2005, pp. 219-222.

SPURIOUS MODE SUPPRESSION IN UHF MICROMECHANICAL EXTENSIONAL WINE-GLASS RING RESONATORS

Yuan Xie, Sheng-Shian Li, Yu-Wei Lin, Zeying Ren, and Clark T.-C. Nguyen

Center for Wireless Integrated Micro Systems
Department of Electrical Engineering and Computer Science
University of Michigan, Ann Arbor, Michigan 48109-2122, USA

ABSTRACT

A geometry-specific excitation configuration has been used to suppress all undesired spurious modes around the center frequencies of stand-alone micromechanical extensional wine-glass ring ("ext. WGR") resonators, previously demonstrated at frequencies up to 1.47-GHz with Q's >2,000 [1]. Using this technique, spurious modes at 406.7, 418, and 419 MHz, normally observed near the resonance of a 415-MHz ext. WGR, have been removed, as have all spurious modes within at least a 50% bandwidth region around the resonance. In removing unwanted modes, this technique solves one of the most encumbering issues with ring-type (as opposed to disk-type [2]) GHz resonators, and paves the way for their use in the micromechanical oscillator and filter circuits targeted for future wireless transceivers [3].

I. INTRODUCTION

Having achieved GHz frequencies and quality factors (Q) > 10,000, even in air [2][4], vibrating micromechanical resonators are becoming attractive candidates for use in the front-end band- or channel-select filter banks sought by multi-band wireless transceiver designers. Among the resonators demonstrated so far above 1 GHz, disk resonators [2] have so far attained the highest frequency-Q products, but ring resonators [1][4][5] are more conducive to lower impedances. Given the importance (or at least perception of importance [3]) of impedance as an encumbering issue for these devices, ring resonators operating in extensional wine-glass or radial modes are of great interest, since their impedances can be tailored independently of their frequencies via proper scaling. Unfortunately, however, ring structures offer up a larger number of spurious modes than disks, and these modes get closer to each other as the impedance of a ring is lowered (i.e., as its size gets larger). The unwanted modes can be as close as a few megahertz from the desired UHF frequency, which is too close for RF front-end applications.

This work describes methods to suppress spurious modes in ring resonators by (1) designing resonator supports to increase vibrational energy loss in unwanted modes; (2) applying forces that accentuate the desired mode shape; and (3) using a detection scheme that suppresses motional currents from undesired modes. Using these techniques, spurious modes at 406.7, 418, and 419 MHz, normally observed near the resonance of a 415-MHz ext. WGR, have been removed, as have all spurious modes within at least a 50% bandwidth region around the resonance.

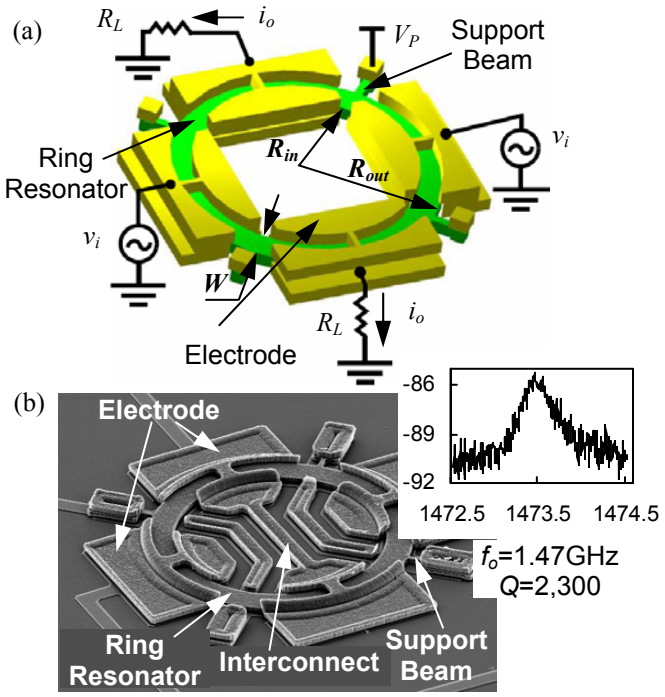

Fig. 1 (a) Perspective-view schematic of an extensional wine-glass ring resonator, identifying key features and a typical drive and sense configuration; and (b) SEM and measured frequency characteristics (from [1]) for a fabricated ext. WGR resonator.

II. DEVICE STRUCTURE AND OPERATION

In the interest of focusing the discussion, this paper takes the ext. WG mode of a ring resonator as the "desired" mode, and treats all other modes as spurious or "undesired". The ext. WGR, depicted in Fig. 1, was first introduced in [1]. As shown in Fig. 1, this device consists of a conductive ring suspended 650 nm above the substrate by tethers attached at extensional wine-glass perimeter nodal points (indicated in the mode shape of Fig. 2(b)). The support tethers are designed with geometries that isolate the resonator structure from its anchors in order to minimize energy losses to the substrate, allowing the structure to retain its highest Q. The ring structure itself is surrounded both inside and outside by drive and sense electrodes spaced only 85 nm from the ring edges. To excite the device, a dc-bias voltage V_P is applied to the conductive ring and an ac voltage v_i to specific drive electrodes. Together, these voltages generate an electrostatic force at the frequency of v_i, given by

$$f_d = \frac{1}{2}(V_P - v_i)^2 \frac{\partial C}{\partial r} \quad (1)$$

that drives the device into resonance vibration when its frequency matches the resonance frequency f_o. In (1), C is the electrode-to-ring overlap capacitance, and $\partial C/\partial r$ is the change in this capacitance per unit radial displacement. Once vibrating, dc-biased (by V_P) time-varying electrode-to-resonator capacitors generate currents that serve as the device output, given by

$$i_o = V_P \frac{dC}{dt} \quad (2)$$

where the direction (i.e., in or out of the electrode terminal) of i_o depends upon the phase of dC/dt. The resonance frequency of an ext. WGR is most accurately specified via simultaneous solution of a rather complicated set of expressions and matrices [1][7], but for intuitive purposes can be specified approximately by

$$f_o = \frac{1}{2W}\sqrt{\frac{E}{\rho(1-\sigma^2)}} \quad (3)$$

where $W = (R_{out} - R_{in})$ is the ring width; and ρ, σ, and E are the density, Poisson ratio, and Young's modulus, respectively, of the structural material. From (3), it is clear that the frequency of the ring can be set independently of its average radius, allowing a designer to set the electrode-to-ring overlap area as large as desired. This, together with the availability of both inner and outer electrodes (as opposed to only an outer electrode in disks), allows single ring resonators to achieve higher electrode-to-resonator overlaps, hence lower impedances, than single disks. (As discussed in [3], however, arrays of these devices are another story.)

III. Spurious Modes and Their Suppression

Unfortunately, although capable of achieving lower impedance than solid disk resonators [2], the ext. WGR and a later radial-mode "hollow disk" ring introduced in [4], both suffer from spurious modes close to their intended resonances. Fig. 2(a)(c)(d) depict some of the more troublesome spurious lateral modes, with theoretically-predicted frequencies as close as 3 MHz to the intended 415 MHz ext. WGR frequency for a ring with an inner radius R_{in} of 32.4μm and an outer radius R_{out} of 42.3μm.

To make matters worse, the separation between intended and spurious modes becomes even smaller as the ring radius increases—a condition that seems to undermine the radius-dependent impedance advantage of a ring structure. For example, ANSYS simulation predicts that for an even larger ring with an outer radius of 100μm, the ext. WGR and radial modes are only 0.7MHz apart—quite problematic if large ring radius is to be used to reduce device impedance [1][5].

Perhaps the best defense against the above problem is to eliminate the undesired modes from the outset. This work attempts to do so by: (1) designing resonator supports to suppress spurious modes; (2) applying forces that accentuate the desired mode shape (in this case, the extensional wine-glass mode shape) while opposing the shapes of other modes; and (3) using a detection scheme that cancels the motional currents of undesired modes. Each of these strategies are now described.

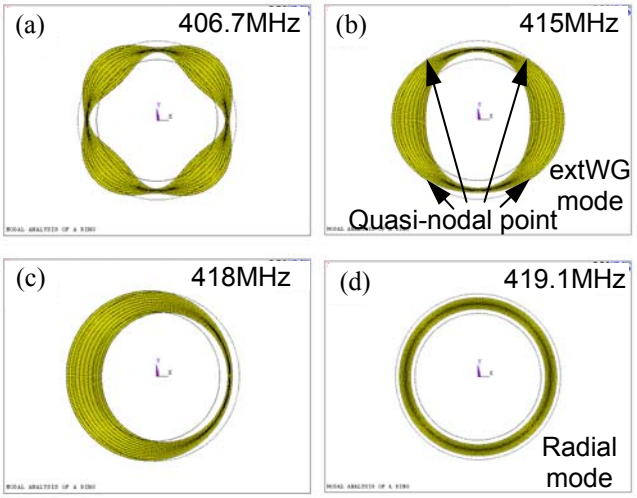

Fig. 2 ANSYS simulated mode shapes of a ring resonator with an inner radius of 32.4μm and an outer radius of 42.3μm. Here, (b) is the desired mode, while (a)(c)(d) are spurious.

A. Mechanical Mode Suppression (Mode Damping)

As has been shown numerous times, the Q of any high stiffness, high frequency resonator is a strong function of the energy per cycle lost through its supports and anchors. Indeed, the micromechanical resonators that presently hold frequency-Q product records at VHF and UHF all do so via isolating support designs that suppress anchor losses [2][4][8][9]. For these resonators, raising the Q of a given mode effectively equates to accentuating that mode relative to other unwanted modes. The opposite approach is also possible, where supports are designed to purposely lower the Q of unwanted modes, thereby suppressing them. Clearly, support design to minimize anchor losses for the desired mode, while maximizing such losses for other mode shapes, constitutes one of the more effective approaches to selecting a desired mode while suppressing others.

The design of Fig. 1(a) does just this by attaching its support tethers to the quasi-nodal points of the ext. WGR and suppressing unwanted modes by physically attenuating their motions. The degree to which other modes can be attenuated depends upon how rigid the tethers appear to their specific motions at their specific frequencies. For example, mode (a) is attenuated the most by the support design of Fig. 1, since the tether attachment locations actually correspond its anti-nodes (i.e., its points of maximum displacement). This mode, in fact, is not even measurable in any of the plots to be presented in Section IV. From Fig. 2, modes (c) and (d) have mode shapes that, again, oppose the support structure, but to a lesser degree than mode (a).

Mode (d), the radial mode, will be most strongly suppressed if the support beams have very small lengths (e.g., less than 1/8-wavelength) or lengths corresponding to an extensional half-wavelength at the radial-mode resonance frequency. In the present design, the support beams are sized to accentuate the ext. WGR mode (as opposed to attenuate the radial mode). In particular, although the support attachment points correspond to nodes in the radial direc-

tion, they are actually not rotational nodes, so rotations still occur at these points. To isolate this rotational motion from the anchors, the support beams are designed to vibrate in a simple-fixed flexural mode at the ext. WGR resonance frequency. At 415 MHz, this entails a support beam length and width of 4.2μm and 1.3μm, respectively. At the 419.1 MHz radial mode resonance frequency, these dimensions correspond to an extensional-mode λ/5—not the half-wavelength required to completely suppress the radial mode, but still enough to provide some attenuation.

In the meantime, the support configuration of Fig. 1 attenuates mode (c) even less than it does (d). In particular, although mode (c)'s radial displacements are opposed somewhat by the support tethers, its rotational displacements are not opposed as strongly, since these rotations are not dissimilar to those of the ext. WGR mode. Thus, mode (c) must be attenuated by some other means.

B. Electrical Mode Suppression

In addition to mechanical damping, electrical means for mode selection are also available. In particular, the phasings between drive electrodes and positioning/biasing of sense electrodes can accentuate one mode while suppressing others. To illustrate, Fig. 3 contrasts three different excitation/detection schemes for the ext. WGR mode in order of increasing ability to suppress spurious modes.

The configuration of Fig. 3(a) drives via the *y*-axis electrodes, and senses along the *x*-axis electrodes. This results in drive forces phase-consistent with all modes of Fig. 2, so this electrode configuration makes no attempt to suppress undesired modes by force tailoring. It, however, does suppress modes (a) and (c) via a sense electrode configuration that cancels their motional currents. In particular, the symmetry of mode (a)'s shape leads to a total capacitance along each sense electrode that remains approximately constant as the ring vibrates, making dC/dt~0, for which the output current is zero according to (2). Furthermore, the mode shape of (c) is such that when a positive dC/dt is generated at the left electrode, an approximately equal but negative dC/dt ensues at the right side, creating equal and opposite motional currents given by (2) that cancel when combined at the sense terminal. The only modes that remain unscathed under this electrode sensing configuration are those for which the dC/dt's over the left and right sense electrodes remain finite and identical at all times, creating a condition where currents from each electrode add at the sense terminal. Fortunately, this includes the desired ext. WGR mode shape of Fig. 2(b). Unfortunately, it also includes the unwanted radial mode (d), as well.

To suppress mode (d), the configuration of Fig. 3(b) uses an orthogonal differential input, with $+v_i$ applied to the *y*-axis electrodes, and $-v_i$ to the left side *x*-axis electrode, to tailor its force phasings so that they oppose some or all of the displacement directions of modes (a) and (d), thereby suppressing them. Unfortunately, with the right side *x*-axis electrode used for sensing, the *x*-axis $-v_i$ drive component is not fully symmetric, so does little to suppress mode (c). Furthermore, the right side *x*-axis sense electrode in Fig. 3(b) does nothing to cancel mode (c)'s motional current.

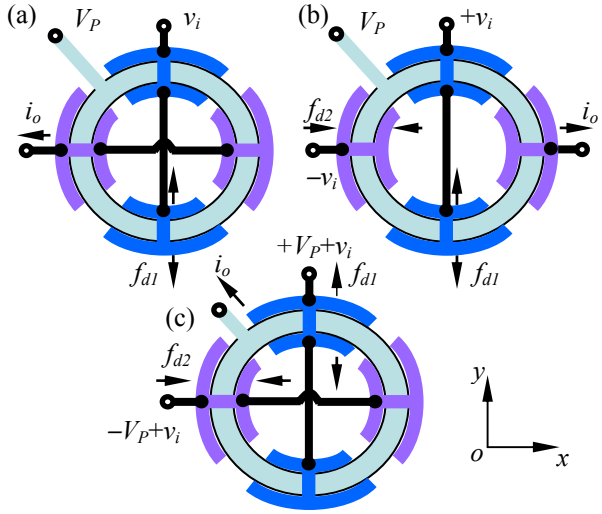

Fig. 3 Excitation/detection scheme: (a) traditional two-port; (b) orthogonal asymmetric differential drive; and (c) orthogonal differential drive, common-mode one-port sense, where the output is taken from the structure itself.

To remedy this problem, the (one-port) scheme of Fig. 3(c) achieves an orthogonal fully differential forcing and sensing configuration by applying $+V_P+v_i$ to the *y*-axis electrodes, $-V_P+v_i$ to the *x*-axis electrodes, and using the ring itself as the current output port (which normally makes it an effective ac ground). With this V_P configuration, when v_i goes positive, the *y*-axis electrodes generate forces proportional to $(V_P+v_i)^2$ that get larger with v_i and pull the ring apart; while the (orthogonal) *x*-axis electrodes generate forces proportional to $(v_i-V_P)^2$ that get smaller with v_i and reduce the pull by these electrodes, effectively imparting an incremental compression. In effect, a differential force acting along orthogonal axes is attained using a single phase v_i and a $\pm V_P$. This orthogonal fully differential forcing configuration now suppresses all spurious modes (a)(c)(d), while accentuating the ext. WGR mode. The scheme of Fig. 3(c) not only attenuates via drive force tailoring, but also further suppresses spurious modes via its one-port common-mode sensing configuration. Here, the output current is sensed directly off the ring, and $\pm V_P$'s are used to cancel the output currents of any *y*-axis asymmetric mode shape, such as mode (c), while preserving those of the ext. WGR mode.

It should be noted that when used in a fully differential application, such as that in [10], a common-mode sense output is not needed. Rather, an orthogonal differential drive *and* sense are required, which can be much more easily realized than Fig. 3(c) by merely applying V_P to the resonator and using the orthogonal electrodes fully differentially.

IV. Experimental Results

To evaluate the effectiveness of the spurious mode suppression techniques described in Section III, each technique was applied to a fabricated 415 MHz ext. WGR resonator, and measurements made under vacuum using a previously described custom-built vacuum chamber [1]. To facilitate output current detection, the configurations of Fig. 3 were modified for actual measurement in order to allow the mixing approach described in [2][6], which greatly enhances the

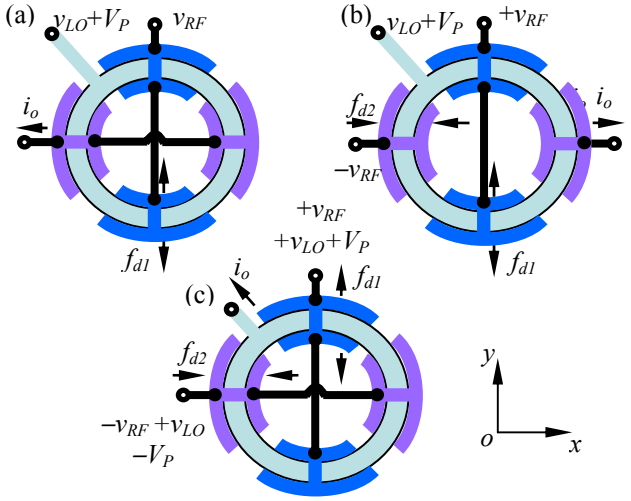

Fig. 4 Mixing measurement setups for each setup in Fig. 3.

detectible output current relative to potentially troublesome feedthrough parasitics. In this mixing approach, a local oscillator signal added to the dc-bias V_P uses capacitive transducer nonlinearity to separate motional currents from feedthrough parasitics in the frequency domain. Fig. 4 presents the mixing-based configurations corresponding to each of the configurations in Fig. 3.

Fig. 5(a)-(c) present frequency spectra measured using the corresponding lettered configuration in Fig. 4. As predicted in Section III, the traditional two-port configuration of Fig. 4(a) excites and senses the ext. WGR mode of Fig. 2(b), while suppressing completely all other modes, except for the radial mode of Fig. 2(d), which is still seen but suppressed somewhat by the support structure. The frequency spectrum of Fig. 5(b) further verifies the prediction of Section III that the orthogonal asymmetric differential excitation scheme with single-ended output of Fig. 4(b) will suppress mode (a) and (d), but not mode (c). Finally, the absence of any spurious modes in Fig. 5(c) verifies that the orthogonal fully differential drive configuration of Fig. 4(c) works as advertised to eliminate all close-in spurious modes, while accentuating the desired ext. WGR mode. Fig. 6 presents a measurement over a much wider frequency span from 300MHz to 500MHz (a 50% bandwidth region) using Fig. 4(c), over which no other modes are observed—an impressive demonstration of mode suppression.

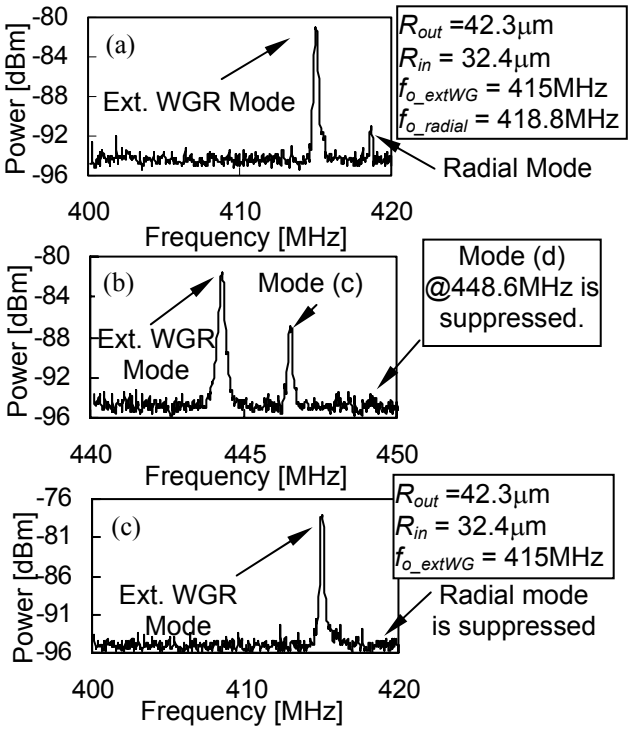

Fig. 5 Frequency spectra measured using corresponding configurations in Fig. 4. The measured resonator in (b) with five ports available is not the same design as in the other two plots, because that device did not have sufficient electrode flexibility to allow the hookup of Fig. 4(b).

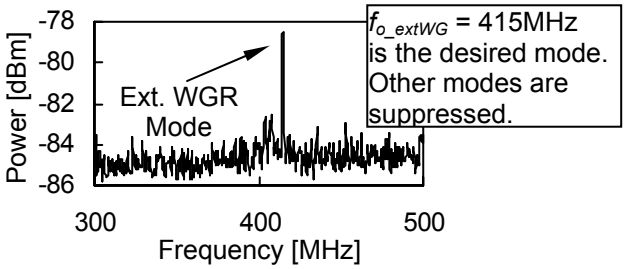

Fig. 6 Frequency spectrum measured using the setup of Fig. 4(c) over a wide frequency span, showing no spurious modes.

V. Conclusions

Through a combination of suspension-derived damping, electrostatic force tailoring, and sense electrode current cancellation, the unwanted spurious modes at 406.7, 418 and 419.1MHz, around the 415 MHz resonance of a UHF micromechanical extensional wine-glass ring resonator have been completely suppressed. In removing unwanted modes, the techniques of this work solve one of the most encumbering issues with ring-type GHz resonators, and pave the way for their use in the micromechanical oscillator and filter circuits targeted for future wireless transceivers [3].

Acknowledgement: This work was supported by DARPA.

References

[1] Y. Xie, *et al.*, "UHF micromechanical extensional wine-glass mode ring resonators," IEDM'03, pp. 953-956.

[2] J. Wang, *et al.*, "1.51-GHz nanocrystalline diamond micromechanical disk resonator with material-mismatched isolating support," MEMS'04, pp. 641-644.

[3] C. T.-C. Nguyen, "Vibrating RF MEMS for next generation wireless apps. (invited)," 2004 IEEE CICC, pp. 257-264.

[4] S.-S. Li, *et al.*, "Micromechanical "hollow-disk" ring resonators," MEMS'04, pp. 821-824.

[5] B. Bircumshaw, *et al.*, "The radial bulk annular resonator: towards a 50Ω filter," Transducers'03, pp. 875-879.

[6] A.-C. Wong, *et al.*, "Micromechanical mixer-filters ("mixlers")," *JMEMS*, vol. 13, no. 1, pp. 100-112, Feb. 2004.

[7] G. Ambati, *et al.*, "In-plane vibrations of annular rings," *J. Sound and Vibration*, vol. 47, no. 3, pp. 415-432, 1976.

[8] K. Wang, *et al.*, "VHF free-free beam high-*Q* μmechanical resonators," *JMEMS*, vol. 9, no. 3, pp. 347-360, Sept. 2000.

[9] M. A. Abdelmoneum, *et al.*, "Stemless wine-glass-mode disk μmech. resonators," MEMS'03, pp. 698-701.

[10] K. Wang, *et al.*, "High-order medium freq. μmechanical electronic filters," *JMEMS*, vol. 8, no. 4, pp. 534-557, Dec. 1999.